

Electronic Resonance and Symmetry in Single-Molecule Inelastic Electron Tunneling

J. R. Hahn, H. J. Lee, and W. Ho

*Laboratory of Atomic and Solid State Physics and Cornell Center for Materials Research, Cornell University,
Ithaca, New York 14853*

(Received 27 April 2000)

Inelastic electron tunneling spectroscopy and microscopy with a scanning tunneling microscope revealed two vibrational modes showing a *decrease* in conductance at ± 82.0 and ± 38.3 mV sample bias for single oxygen molecules chemisorbed on the fourfold hollow sites of Ag(110) surface at 13 K. The spatial distribution of the vibrational intensities exhibited π_g -orbital (perpendicular to surface) symmetry of O₂ with the molecular axis along the [001] direction. These results are attributed to resonant inelastic electron tunneling.

PACS numbers: 68.35.Ja, 07.79.Cz, 34.50.Ez, 61.16.Ch

Vibrational spectroscopy of molecules adsorbed on a solid surface is a powerful tool for chemical identification and for understanding the nature of chemical bonding and the local chemical environment. Inelastic electron tunneling spectroscopy using a scanning tunneling microscope (STM-IETS) [1] makes it possible to perform vibrational spectroscopy on a single molecule. In addition to the vibrational spectra, the high spatial resolution achieved in topographic imaging and vibrational intensity mapping provides insights into the correlation between the electronic structure and vibrational excitation of adsorbed molecules. The inelastic electron tunneling phenomenon in STM-IETS involves the coupling and energy transfer between tunneling electrons and the vibrational modes. Therefore, these experiments can reveal the electronic states of the adsorbate and substrate through which inelastic tunneling occurs. The observation of new "tunneling-active" vibrational modes also broadens the usefulness of STM-IETS as an analytical technique, and leads to a better understanding of electron-vibration coupling which is basic to many chemical processes.

Oxygen on silver has served as a model system for studying gas-surface interactions because of its catalytic importance as well as its distinct states of adsorption at different temperatures. The O₂ molecule is physisorbed on the Ag(110) surface below 40 K and becomes chemisorbed between 40 and 150 K [2]. The molecularly chemisorbed state has been studied by various techniques [3–7]; however, conflicting views still exist regarding the nature of the state. Molecular O₂ chemisorbs parallel to the surface [2,4,6] and the O-O bond is considerably weakened by a charge transfer between the silver and the O₂ 1 π orbitals [2,3]. Two vibrational modes, the O-O stretch and the symmetric stretch of O₂-Ag, have been observed by electron energy loss spectroscopy (EELS) [3,4].

In this Letter, we report single-molecule vibrational spectroscopy and microscopy of O₂ chemisorbed on Ag(110) using STM-IETS. The topographic images of O₂ were obtained with bare and CO-terminated tips. Two vibrational modes, leading to a decrease in ac conduc-

tance, were observed. The vibrational intensities for both modes were found to be spatially localized and exhibited a striking symmetry, which revealed the electronic state responsible for the inelastic tunneling process.

Experiments were carried out using a homemade, variable temperature STM [8], housed inside an ultrahigh vacuum chamber with a base pressure of 2×10^{-11} Torr. The Ag(110) sample was cleaned by 500 eV Ne ion sputtering and 693 K annealing cycles. Etched polycrystalline tungsten tips were also sputtered and annealed prior to use. The O₂ molecules were dosed through a capillary array and adsorbed on the sample at 45 K in order to ensure molecular chemisorption. The O₂ coverage was below 0.01 ML. The sample and the STM were then cooled down to 13 K for spectroscopy and microscopy. A very small number of CO molecules (<0.001 ML) were also adsorbed on the surface either at 45 or 13 K. A CO molecule can be transferred to the tip, enabling atomically resolved imaging [9].

Two types of O₂ chemisorbed on Ag(110) between 45 and 75 K were revealed in the STM images [10]. This observation is consistent with first principles calculations which showed the O₂ with its bond axis oriented along the [001] direction to be slightly more stable (by 0.04 eV for a relaxed Ag surface) than the other type with its bond axis oriented along the [1 $\bar{1}$ 0] direction. The slightly more stable O₂ species [shown in Figs. 1(a) and 1(c)] was found to reproducibly dissociate into two oxygen atoms by tunneling electrons with energy 0.02 eV higher than for the other type. It was further determined that a dissociation pathway of the more stable O₂ involved the conversion to the other species and then the two oxygen atoms were always found to lie along the [1 $\bar{1}$ 0] direction [10]. These results suggest that the molecular axis of the more stable O₂ lies along the [001] direction. This geometry is also consistent with the spatial symmetry of the electronic orbital and vibrational intensity of the O₂/Ag(110) species presented in this paper, hereafter referred to simply as O₂.

The topographical image of O₂ exhibits an oval-shaped depression with a maximum depth of 0.4 Å [Figs. 1(a) and 1(b)]. With a CO-terminated tip, the image was modified,

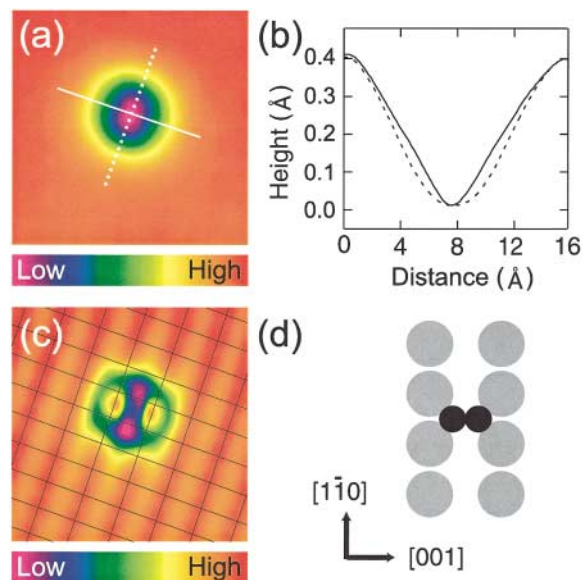


FIG. 1 (color). STM images, $25 \text{ \AA} \times 25 \text{ \AA}$, of single O_2 molecule chemisorbed on $\text{Ag}(110)$. (a) Topographic image obtained with a bare tip at 70 mV sample bias and 1 nA tunneling current. (b) Cross sections of (a) taken along the $[001]$ (solid line) and $[1\bar{1}0]$ (dashed line) directions. (c) Atomically resolved STM topographic image obtained with a CO-terminated tip at 70 mV sample bias and 1 nA tunneling current. Grid lines are drawn through the silver surface atoms. (d) Schematic diagram of the adsorption site. The small black circles represent oxygen atoms and the large gray circles silver atoms.

including the appearance of two prominent protrusions [Fig. 1(c)]. In addition, atomic resolution of the $\text{Ag}(110)$ surface was obtained and allowed the determination of the O_2 adsorption site as the fourfold hollow, shown schematically in Fig. 1(d).

Vibrational spectra (Fig. 2) were obtained by STM-IETS for chemisorbed $^{16}\text{O}_2$ (curve *a*) and $^{18}\text{O}_2$ (curve *b*) on $\text{Ag}(110)$. The spectrum taken over $\text{Ag}(110)$ surface (curve *c*) is also shown for comparison. The difference spectra (curves *a-c* and *b-c*) reveal two dips at positive bias and two peaks at negative bias. The spectral shifts from isotopic substitution were resolved. The positions of the peaks and dips were determined by fitting the spectra obtained with a higher resolution (0.5 mV step) in the region of a peak or a dip to a Gaussian function. Positions of the peaks at negative sample bias were not measurably different in magnitude from those of the dips at positive bias.

The feature at 82.0 (76.6) meV for $^{16}\text{O}_2$ ($^{18}\text{O}_2$) is assigned to the O-O stretch vibration, in close agreement with the values of 80 meV for $^{16}\text{O}_2$ obtained by EELS [3,4]. The symmetric O_2 -Ag stretch (30 meV for $^{16}\text{O}_2$) [3,4] was not observed. The vibrational feature at 38.3 (35.8) meV for $^{16}\text{O}_2$ ($^{18}\text{O}_2$) is attributed to the antisymmetric O_2 -Ag stretch vibration (discussed below). This mode has not been reported in previous experimental and theoretical vibrational analyses of O_2 chemisorbed on $\text{Ag}(110)$. The dips (peaks) at positive (negative) bias in the d^2I/dV^2

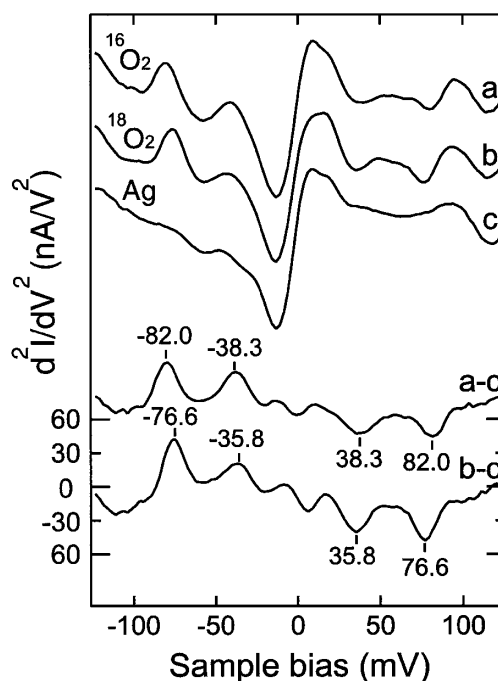


FIG. 2. Single molecule vibrational spectra obtained by STM-IETS for $^{16}\text{O}_2$ (curve *a*), $^{18}\text{O}_2$ (curve *b*), and the clean $\text{Ag}(110)$ surface (curve *c*). The O_2 spectra were taken over a position 1.6 \AA from the molecular center along the $[001]$ axis. The spectra displayed are averages of multiple scans from -125 mV to $+125 \text{ mV}$ and back down. Dwell time of 300 ms per 2.5 mV step and 7 mV rms bias modulation at 200 Hz were used for recording the spectra. The number of scans is 122, 321, and 100 for *a*, *b*, and *c*, respectively. The difference spectra (curve *a-c*, curve *b-c*) are shown. The line markers indicate the positions of the vibrational modes. The relative conductance changes, $\Delta\sigma/\sigma$ where $\sigma = dI/dV$, are $-2.7 \pm 0.8(-2.4 \pm 0.4)\%$ and $-1.8 \pm 0.7(-1.1 \pm 0.3)\%$ at negative sample bias, for the stretch vibration of $^{16}\text{O}_2$ ($^{18}\text{O}_2$) and antisymmetric stretch of $^{16}\text{O}_2$ ($^{18}\text{O}_2$)-Ag, respectively. The corresponding changes at positive sample bias are $-2.3 \pm 0.6(-1.6 \pm 0.1)\%$ and $-1.9 \pm 0.8(-1.3 \pm 0.1)\%$.

spectra of O_2 indicate that the excitation of molecular vibrations causes a decrease in the ac tunneling conductance (dI/dV). This is in contrast with peaks (dips) at positive (negative) bias, i.e., an increase in dI/dV , reported to date for other molecular systems: acetylene [1,11], CO [12], ethynyl [13], and pyridine [14]. This difference has important theoretical implications for understanding the mechanism of STM-IETS.

When an electronic resonance of the adsorbate overlaps the Fermi level of the substrate, the onset of vibrational excitation may lead to an overall decrease in the ac tunneling conductance due to the suppression of elastic tunneling [15]. The decrease in the ac conductance was predicted for the case of a resonant tunneling process in STM; chemisorbed CH_3CN on Rh particles and O_2 on $\text{Pt}(111)$ were given as potential examples [15]. Recently, Lorente and Persson [16] have determined that, for acetylene on $\text{Cu}(100)$, the change in the elastic conductance is negative, whereas that of the inelastic conductance is positive at the

threshold for a vibrational excitation. In this case of non-resonant tunneling, an overall increase in ac conductance was calculated, in agreement with the experiment [1,11].

Further insights into the mechanism of STM-IETS can be obtained from spatially resolved vibrational spectra shown in Fig. 3 for the O-O stretch vibration. The maximum intensity for the O-O stretch vibration occurred in the spectrum taken with the tip positioned at point *e*, 1.6 Å away from the center of molecule along the [001] direction. None of the spectra recorded along the $[1\bar{1}0]$ axis of the molecule (*i-m*) showed measurable vibrational intensity.

The spatial distribution of the STM-IETS intensity can also be probed by recording the topographic and vibrational images simultaneously [1,11,12]. Vibrational microscopy images of a single $^{18}\text{O}_2$ molecule were obtained at sample biases of -76.6 mV [Fig. 4(c)] and -35.8 mV [Fig. 4(e)] with a bare metallic tip. Simultaneous topographic and vibrational imaging allows the spatial localization of the inelastic tunneling signal to be compared with the molecular topography. The area of the vibrational images [Figs. 4(c) and 4(e)] was rescanned in constant current mode with a CO-terminated tip [Fig. 4(a)]. No significant difference was observed between topographical images taken at positive and negative sample biases. Cross sections along the $[1\bar{1}0]$ (dashed line) and [001] (solid line) directions reveal quantitative variations in the topography and vibrational intensity. It is only with a CO-terminated tip that the two protrusions in the topographic images are resolved, as shown in Figs. 1(c) and 4(a). In a complementary way, the vibrationally inelastic tunneling process highlights the two protrusions associated with the O_2 electronic structure. The images of Ag atoms and adsorbed CO and O obtained with a CO-terminated tip are azimuthally symmetric, which permits the assignment of the protrusions in O_2 images to the electronic structure of O_2 as opposed to that of the tip.

The spatial distribution of the vibrational intensity for both modes exhibits the symmetry of the 1π orbital. The two intensity maxima occur symmetrically along the [001]

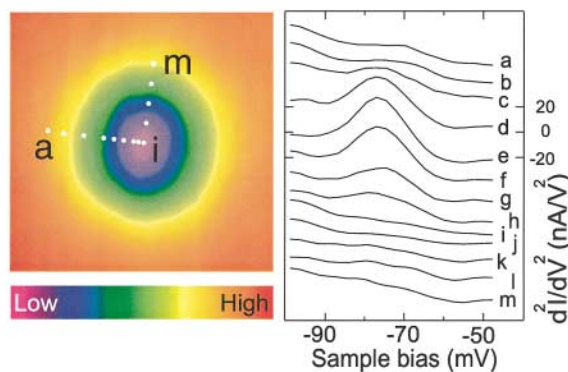


FIG. 3 (color). Spatially resolved, background subtracted spectra for the stretch vibration of $^{18}\text{O}_2$ on Ag(110). The spectra *a-i* were obtained along the [001] direction and the spectra *i-m* along the $[1\bar{1}0]$ direction. The number of scans for each spectrum is 30.

direction, 1.6 Å away from the molecular center, which suggests the dominance of the $1\pi_g^\perp$ orbital (perpendicular to surface and along the [001] direction) of O_2 in the inelastic tunneling process. The symmetry of the vibrational images is preserved for the corresponding vibrations at $+76.6$ and $+35.8$ mV except that the vibrational intensities are negative (dips instead of peaks in d^2I/dV^2). These results at positive and negative biases indicate that the $1\pi_g^\perp$ orbital is partially occupied.

The position and line shape of the spectral features and the symmetry of the vibrational images are the same for bare and CO-terminated tips. The topographic features of

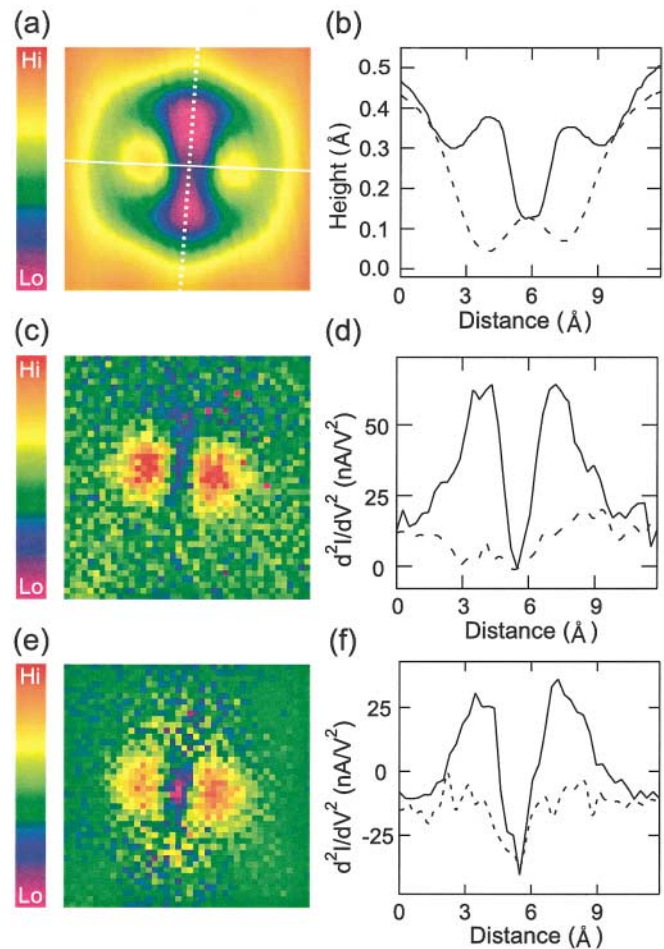


FIG. 4 (color). Comparison of the topographic image of $^{18}\text{O}_2$ and the spatial distribution of STM-IETS intensity for the two vibrational modes. (a) $12 \text{ \AA} \times 12 \text{ \AA}$ topographic image taken at sample bias of 70 mV and tunneling current of 1 nA with a CO-terminated tip. The image was smoothed. (b) Cross sections of (a) taken along the [001] (solid line) and the $[1\bar{1}0]$ (dashed line) directions. (c) Vibrational image obtained at -76.6 mV sample bias, corresponding to the O-O stretch vibration. (d) Cross sections of (c) taken along the two directions shown in (a). (e) Vibrational image obtained at -35.8 mV bias, corresponding to the antisymmetric stretch of O_2 -Ag. This vibrational image is the average of four scans. (f) Cross sections of (e) taken along the two directions shown in (a). (c) and (e) were obtained with a bare metallic tip. The raw data, $12 \text{ \AA} \times 12 \text{ \AA}$ area, are shown at a resolution of $0.3 \text{ \AA}/\text{pixel}$.

an adsorbate molecular orbital can, however, be amplified with a CO-terminated tip [17]. The two protrusions in the topographic image of O₂ obtained with the CO-terminated tip indicate a high local density of states which can be associated with the $1\pi_g^\perp$ molecular orbital about the Fermi level. Filling of this resonance upon chemisorption is associated with an elongation of the O-O bond axis [2,3]. Similarly, the energy associated with a nonequilibrium charge distribution created by tunneling electrons could be effectively transferred to vibrational degrees of freedom.

The vibrational feature at 38.3 (35.8) meV for ¹⁶O₂ (¹⁸O₂) could be either the antisymmetric O₂-Ag stretch or the hindered rotation of O₂ parallel to the surface. The symmetric O₂-Ag(110) stretch is ruled out because its vibration energy is 30 meV for ¹⁶O₂ [3,4]. The symmetry of the vibrational image is helpful in assigning this vibrational mode. Theoretical analysis has shown that the symmetry of the vibrational image is determined by the symmetries of electronic states at the Fermi level and the vibrational motion [16]. For O₂ on Ag(110), the $1\pi_g^\perp$ orbital is antisymmetric (symmetric) with respect to the mirror plane perpendicular to the surface and containing the $[1\bar{1}0]$ ([001]) axis. For the antisymmetric O₂-Ag stretch motion, the symmetries with respect to the two mirror planes are the same as those of the O₂ $1\pi_g^\perp$ orbital. This leads to a totally symmetric vibrational image with respect to the two mirror planes, in agreement with the experimental results shown in Figs. 4(e) and 4(f). In contrast, the hindered rotation parallel of O₂ to the surface is antisymmetric while the $1\pi_g^\perp$ orbital is symmetric with respect to the mirror plane including the [001] axis; the vibrational image should then exhibit a nodal plane along this mirror plane, which is in sharp contrast to the large intensity observed in Figs. 4(e) and 4(f). However, the internal stretch vibration of O₂ is symmetric with respect to the mirror plane containing the $[1\bar{1}0]$ axis, while the $1\pi_g^\perp$ orbital is antisymmetric. Thus this mirror plane should be a nodal plane for this mode. The negligible intensity observed for the inelastic tunneling signal in this plane, as shown in Figs. 4(c) and 4(d), is consistent with this symmetry analysis.

While the $1\pi_g^\parallel$ orbital also overlaps the Fermi level, symmetry considerations rule out its contribution to the excitation of the internal O-O stretch and the antisymmetric O₂-Ag stretch. Although the excitation of the hindered rotation involving the $1\pi_g^\parallel$ is symmetry allowed, the STM topographic image in Fig. 4(a) suggests the dominant participation of the $1\pi_g^\perp$ orbital. Neither orbital is symmetry allowed in the excitation of the symmetric O₂-Ag stretch.

Similar analyses disfavor the orientation of the O₂ axis along the $[1\bar{1}0]$ direction.

Two vibrational modes were observed for O₂ chemisorbed on Ag(110) and the excitation of each mode led to a decrease in the ac conductance. The spatial distribution of the inelastic tunneling intensity exhibited a striking symmetry which is attributed to a resonant inelastic tunneling process through the $1\pi_g^\perp$ orbital of O₂. With a CO-terminated tip, it was possible to determine the O₂ binding site and reveal the molecular orbital involved in the inelastic tunneling. These experiments extend STM-IETS to an adsorbate of great fundamental and practical interest. The nature of these vibrational modes and images should further stimulate theoretical development and fundamental understanding of STM-IETS.

We are grateful to M. Persson and N. Lorente for insightful discussions. This research was supported by the U.S. Department of Energy, Division of Chemical Science, Office of Basic Energy Sciences, Office of Energy Research under Grant No. DE-FG02-91ER14205.

-
- [1] B. C. Stipe, M. A. Rezaei, and W. Ho, *Science* **280**, 1732 (1998).
 - [2] P. A. Gravil, D. M. Bird, and J. A. White, *Phys. Rev. Lett.* **77**, 3933 (1996).
 - [3] B. A. Sexton and R. J. Madix, *Chem. Phys. Lett.* **76**, 294 (1980).
 - [4] C. Backx *et al.*, *Surf. Sci.* **104**, 300 (1981).
 - [5] M. A. Barteau and R. J. Madix, *Chem. Phys. Lett.* **97**, 85 (1983).
 - [6] D. A. Outka *et al.*, *Phys. Rev. B* **35**, 4119 (1987).
 - [7] F. Bartolucci *et al.*, *Phys. Rev. Lett.* **80**, 5224 (1998).
 - [8] The STM is a variation of the one described in B. C. Stipe, M. A. Rezaei, and W. Ho, *Rev. Sci. Instrum.* **70**, 137 (1999).
 - [9] H. J. Lee and W. Ho, *Science* **286**, 1719 (1999).
 - [10] J. R. Hahn and W. Ho (unpublished).
 - [11] B. C. Stipe, M. A. Rezaei, and W. Ho, *Phys. Rev. Lett.* **82**, 1724 (1999).
 - [12] L. J. Lauhon and W. Ho, *Phys. Rev. B* **60**, R8525 (1999).
 - [13] L. J. Lauhon and W. Ho, *Phys. Rev. Lett.* **84**, 1527 (2000).
 - [14] L. J. Lauhon and W. Ho, *J. Phys. Chem. A* **104**, 2463 (2000).
 - [15] B. N. J. Persson and A. Baratoff, *Phys. Rev. Lett.* **59**, 339 (1987); B. N. J. Persson, *Phys. Scr.* **38**, 282 (1988).
 - [16] N. Lorente, M. Persson, L. J. Lauhon, and W. Ho (unpublished).
 - [17] M.-L. Bocquet, J. Cerdá, and P. Sautet, *Phys. Rev. B* **59**, 15437 (1999).